Magnetic Resonance in Medicine 79:224–233 (2018)

# Acceleration of ASL-Based Time-Resolved MR Angiography by Acquisition of Control and Labeled Images in the Same Shot (ACTRESS)

Yuriko Suzuki [1,2]* Noriyuki Fujima,[3] Tetsuo Ogino,[2] James Alastair Meakin,[4] Akira Suwa,[2] Hiroyuki Sugimori,[5] Marc Van Cauteren,[6] and Matthias J. P. van Osch[1]

**Purpose:** Noncontrast 4D-MR-angiography (MRA) using arterial spin labeling (ASL) is beneficial because high spatial and temporal resolution can be achieved. However, ASL requires acquisition of labeled and control images for each phase. The purpose of this study is to present a new accelerated 4D-MRA approach that requires only a single control acquisition, achieving similar image quality in approximately half the scan time.

**Methods:** In a multi-phase Look-Locker sequence, the first phase was used as the control image and the labeling pulse was applied before the second phase. By acquiring the control and labeled images within a single Look-Locker cycle, 4D-MRA was generated in nearly half the scan time of conventional ASL. However, this approach potentially could be more sensitive to off-resonance and magnetization transfer (MT) effects. To counter this, careful optimizations of the labeling pulse were performed by Bloch simulations. In in-vivo studies arterial visualization was compared between the new and conventional ASL approaches.

**Results:** Optimization of the labeling pulse successfully minimized off-resonance effects. Qualitative assessment showed that residual MT effects did not degrade visualization of the peripheral arteries.

**Conclusion:** This study demonstrated that the proposed approach achieved similar image quality as conventional ASL-MRA approaches in just over half the scan time. **Magn Reson Med 79:224–233, 2018.** 

**Key words:** Time-resolved MR angiography (MRA); noncontrast 4D-MRA; arterial spin labeling (ASL); hyperbolic secant (HS) pulse; FOCI pulse

## INTRODUCTION

Evaluation of cerebrovascular hemodynamics provides crucial information for accurate diagnosis, treatment selection, and follow-up of diseases such as arteriovenous malformation, arteriovenous fistula, and steno-occlusive disease. Recently, there has been an increasing number of clinical reports using arterial spin labeling (ASL) for noncontrast-enhanced (CE) magnetic resonance angiography (MRA) (1–6), mainly due to the possibility of time-resolved (4D) MRA as well as vessel specificity by restricting the labeling to a single vessel (7,8).

4D-MRA can be achieved by acquiring images with different postlabeling delays (PLDs), for example, by using a Look-Locker readout (9). The benefits of 4D-MRA using ASL is that injection of the contrast agent is not required and that both high temporal and spatial resolution can be achieved. Unlike CE-MRA, which must capture the quick first passage of the contrast agent and therefore suffers from a compromise between temporal and spatial resolution, labeling of arterial blood can be repeated until sufficient data are acquired to achieve both high temporal and spatial resolution, thus enabling detailed visualization of arterial flow hemodynamics by ASL. To achieve this advantage, ASL-based 4D-MRA usually requires a longer acquisition time than CE-MRA. A second reason for the longer acquisition time of ASL-based 4D-MRA is that ASL techniques require the acquisition of two images: one in which the arterial blood is inverted (labeled image) and in the other in which the arterial blood is not inverted (control image). By subtraction of these two images, the background static tissue signal is cancelled out and the inflow of the labeled arterial blood is visualized. The mean acquisition time of previously reported ASL-based 4D-MRA is approximately 7 minutes (5 min–8.5 min) (1–6), which is not always fast enough to enable its use in clinical protocols.

In this paper, we present a novel, ASL-based 4D-MRA technique, named *ACTRESS* (ACquisition of conTRol and labEled image in the Same Shot), which nearly halves the acquisition time by restricting image acquisition to only the labeled condition. Subtraction can be performed by shifting

[1]C.J. Gorter Center for High Field MRI, Department of Radiology, Leiden University Medical Center, Leiden, The Netherlands.

[2]Philips Electronics Japan, Ltd., Healthcare, Tokyo, Japan.

[3]Department of Diagnostic and Interventional Radiology, Hokkaido University Hospital, Hokkaido, Japan.

[4]Diagnostic Image Analysis Group, Radboud University Medical Center, Nijmegen, The Netherlands.

[5]Faculty of Health Sciences, Hokkaido University, Hokkaido, Japan.

[6]Philips Healthcare, Asia Pacific, Tokyo, Japan.

*Correspondence to: Yuriko Suzuki, C.J. Gorter Center for High Field MRI, Department of Radiology, Leiden University Medical Center (LUMC), C3-Q, Albinusdreef 2, 2333 ZA Leiden, The Netherlands. E-mail: y.suzuki@lumc.nl.

COI: Yuriko Suzuki and James A. Meakin are former employees of Philips. Tetsuo Ogino, Akira Suwa, and Marc Van Cauterenare are currently employed by Philips.

The copyright line for this article was changed on 21 March 2018 after original online publication.

Received 24 October 2016; revised 19 January 2017; accepted 12 February 2017

DOI 10.1002/mrm.26667

Published online 20 March 2017 in Wiley Online Library (wileyonlinelibrary.com).

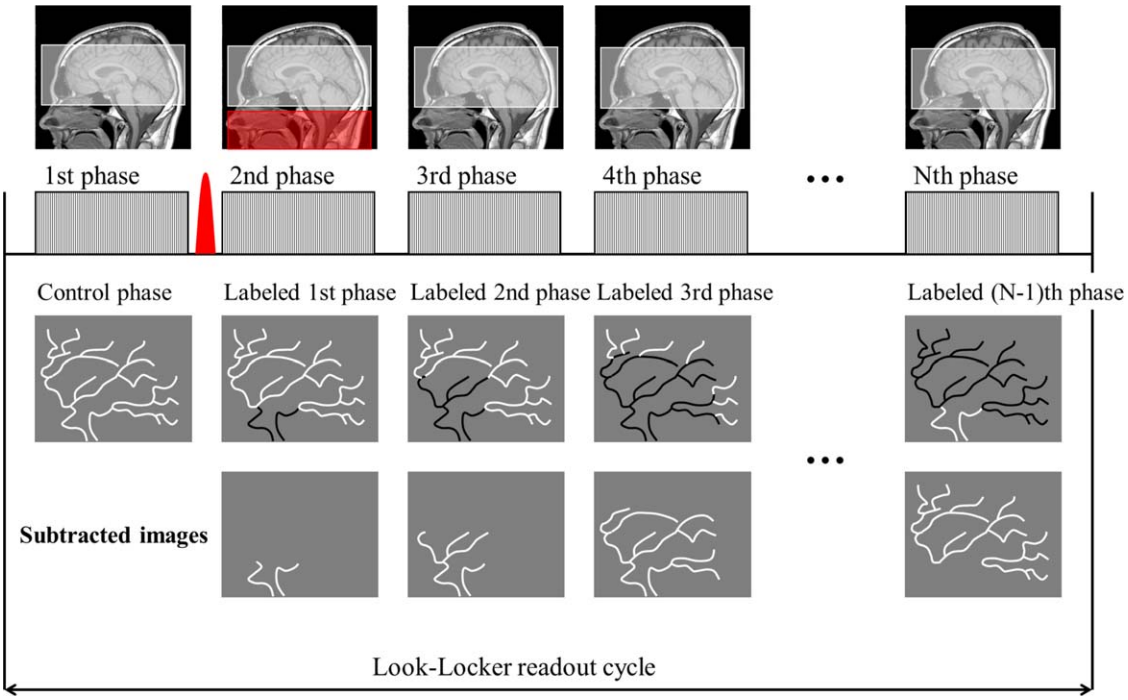


FIG. 1. Basic sequence diagram of ACTRESS (acquisition of control and labeled images in the same shot) approach. A spatially selective labeling pulse is applied prior to the second phase readout, whereas the first phase is employed as the control image. By subtracting all labeled images from the single control image, 4D MR-angiography images are generated.

the labeling pulse to the second phase of the Look-Locker readout and using the first phase as the control image (Fig. 1). However, this approach potentially could induce several artefacts because the subtraction is performed between images acquired in different phases of the Look-Locker readout. Moreover, the control image acquired with this approach might not perfectly cancel out the magnetization transfer (MT) effects, unlike conventional ASL sequences designed to keep label and control images as identical as possible with a similar level of MT effects.

The purpose of this paper is to optimize ACTRESS MRA so that it enables generation of 4D-MRA images of a similar quality to the conventional ASL sequence in nearly half the scan time while avoiding possible artefacts caused by the absence of the separate acquisition of control images. This approach can significantly improve the clinical usability of 4D-ASL due to shorter scan times, which also reduces the occurrence of motion artefacts associated with longer scan duration.

## METHODS

### Introduction of the ACTRESS-Sequence

The principle of ACTRESS-MRA is illustrated in Figure 1. The sequence consists of a 3D multi-shot, multi-phase (multi-PLD) Look-Locker readout in combination with a spatially selective labeling pulse, which is applied prior to the readout of the second phase. It is assumed that the image acquired in the first phase does not have a contribution from labeled blood and therefore can be employed as a control image. In the second and later phases, arterial blood that has been inverted by the labeling pulse will flow into the arterial system, thereby reducing the signal from blood. 4D-MRA images can be generated by subtracting all labeled images (2nd–Nth phase) from the single control image, that is, the first phase. By choosing a long-enough cycle duration, all labeled blood has left the arterial system before the next control phase is acquired. The ACTRESS approach acquires all images necessary to generate 4D-MRA in approximately half the scan time of a conventional ASL approach because by employing the first phase as control image it is no longer necessary to acquire a full, separate set of control images.

For this approach to render similar image quality to the conventional ASL approach, the signal from static tissue should be constant over all phases so that the signal from static tissue will cancel upon subtraction between the first phase image and all subsequent phases. To be more specific, the spatially selective labeling pulse played out before the second readout should have no or minimal influence on the imaging volume. However, when a labeling pulse is applied proximal to the imaging volume, the labeling pulse might affect off-resonant magnetization within the imaging region, depending on the bandwidth (BW) of the labeling pulse and applied slab-selection gradient strength during the pulse, which combined will be referred to as *off-resonance effects* in this paper. When keeping the labeling thickness equal, a radiofrequency (RF) pulse with narrower BW will be combined with a smaller selection gradient, thereby leading to a smaller frequency difference between labeling and imaging regions and thus severer off-resonance effects on imaging region. Possible regions of off-resonance effects include fat and tissue surrounding the paranasal sinuses. Such an influence would result in changes of the static tissue signal after the labeling pulse and recovery in the following phases, leading to subtraction artefacts. In a conventional ASL sequence, such off-resonance effects are avoided by saturating the imaging slices before and after the labeling pulse.

For ACTRESS, however, saturation pulses cannot be used because the signal from static tissue should be as constant as possible over all phases to avoid subtraction artefacts. Similarly, on-resonant tissue can show subtraction artefacts when the inversion profile of the labeling pulse is not sharp enough and the tissue magnetization inside the imaging volume is directly affected by the labeling pulse. Finally, MT effects from the labeling pulse could affect the static tissue signal. In conventional ASL, MT effects are eliminated by using a noninverting control pulse with the same RF power for the control condition so that MT effects will be similar between label and control images and therefore subtracted out. For pulsed ASL (PASL) techniques, application of a postlabeling saturation pulse helps to eliminate residual MT effects even further. However, to minimize MT effects in ACTRESS-MRA for which no RF pulse is applied for the control condition and a postlabeling saturation pulse cannot be applied, RF energy for the labeling pulse should be kept as low as possible. Considering all these potential issues, the labeling RF pulse should be optimized to 1) exhibit minimal off-resonance; 2) exhibit minimal MT effects; 3) provide an excellent labeling efficiency; and 4) provide a sharp profile. In this study, we will consider both hyperbolic secant (HS) (10) as well as frequency offset corrected inversion (FOCI) (11) pulses for performing the labeling.

### Optimization of the Labeling RF Pulse

The HS inversion pulse is one of the most commonly used adiabatic labeling pulses for PASL. It enables uniform inversion over a wide range of $B_1$ amplitudes and can be described by

$$B_1^{HS}(t) = [A_0 \mathrm{sech}(\beta t)]^{1+i\mu}, \quad [1]$$

in which $A_0$ is the maximum $B_1$ field; $\beta$ is the angular frequency that determines the truncation level; and $\mu$ is a dimensionless scaling parameter that defines the degree of phase modulation (12,13). The BW of the HS inversion pulse can be calculated to be

$$\Delta f = \mu\beta/\pi. \quad [2]$$

For convenience of RF pulse implementation, the parameter $\beta_{norm}$ was introduced (defined as

$$\beta_{norm} = \beta^* RF_{dur}/2, \quad [3]$$

with $RF_{dur}$ the duration of the RF pulse in seconds).

A disadvantage of the HS pulse is that the BW is rather narrow and therefore is prone to exert large off-resonance effects, which therefore might be less ideal for our single acquisition approach. The FOCI pulse is a modification of the HS inversion pulse (11,14–16), which provides a sharper inversion profile as well as a broader BW by multiplying the RF amplitude, frequency modulation, and gradient amplitude with an additional modulation function $\alpha(t)$,

$$\begin{aligned} A^{FOCI}(t) &= \alpha(t) \times A^{HS}(t) \\ \Delta\omega^{FOCI}(t) &= \alpha(t) \times \Delta\omega^{HS}(t) \\ G^{FOCI}(t) &= \alpha(t) \times G^{HS} \\ \alpha(t) &= \begin{cases} \cosh(\beta t) & when\ \cosh(\beta t) < \alpha_{max} \\ \alpha_{max} & otherwise \end{cases}, \end{aligned} \quad [4]$$

in which $G^{HS}$ is the selection gradient amplitude used for the HS pulse. In this study, an additional Gaussian modulation is applied to the amplitude modulation aiming for further improvement of the slab profile,

$$A^{FOCI}(t) = \alpha(t) \times A^{HS}(t) \times \exp(-GG2 \times t^2), \quad [5]$$

in which GG2 is a parameter that defines the strength of Gaussian modulation.

Bloch equation simulations were performed in MatLab (MathWorks, Natick, MA, USA) using the maximum $B_1$ amplitude of 13.47 μT allowed on our clinical 3.0 telsa (T) scanner. The inversion profile, off-resonance effects, and labeling efficiency of HS and FOCI pulses were investigated while optimizing the RF pulse parameters; $\beta_{norm}$, $\mu$ and RF integral (defined as

$$\text{RF integral} = \gamma \int_0^{RF\,dur} A(t)dt, \quad [6]$$

corresponding to the RF energy needed to achieve a certain flip angle by a simple nonadiabatic RF pulse) for both the HS and FOCI pulses, and $\alpha_{max}$ and GG2 for the FOCI pulse. The time-varying BW of FOCI pulse $\Delta f^{FOCI}(t)$ was calculated from the time-varying gradient $G^{FOCI}(t)$, the labeling slab thickness $\Delta z$, and gyromagnetic ratio $\gamma$,

$$\Delta f^{FOCI}(t) = \gamma G^{FOCI}(t)\Delta z, \quad [7]$$

and its mean value was defined as the effective BW of the FOCI pulse to reduce the resulting off-resonance effects. The default settings on our scanner for $\beta_{norm}$, $\mu$, and RF integral of the HS labeling pulse for the signal targeting with alternating radio frequency (STAR) sequence (17) are 4.0, 5.0, and 850, respectively. These values were used for comparison and will be referred to as *default settings*. In this simulation, the labeling slab thickness was set to 100 mm, and the $T_1$ and $T_2$ value of 1,450 ms and 85 ms, which were approximate mean value of gray matter and white matter in 3T (18), were used.

### In Vivo Healthy Volunteer Study

The study was approved by the local institutional review board, and all volunteers provided written informed consent before inclusion into this study. A total of six volunteers (male = 2, female = 4, mean age = 31 years [range,19–62 years]) without known cerebrovascular disease participated in the study.

Following the results of the Bloch equation simulation (see Results/Discussion section), an in vivo healthy volunteer study was performed using the optimized HS- and FOCI-labeling pulses focused on finding the optimal inversion thickness of the labeling slab. Also, the images acquired with the ACTRESS sequence were compared to a traditional ASL-based 4D-MRA sequence (STAR), with similar imaging parameters.

The thickness of the labeling slab was set to 80, 100, 120, 160, and 200 mm, whereas the gap between the labeling and imaging volume was fixed at 20 mm. Care was taken to select the appropriate polarity of the volume selection gradient of the labeling pulse to avoid off-resonance effects of the fat within the imaging volume.

Table 1
RF Parameters Used in the Bloch Equation Simulation (a) and In Vivo Study (b)

| | $\beta_{norm}$ | $\beta$ ($s^{-1}$) | $\mu$ | $\alpha_{max}$ | GG2 | RF Integral | BW (Hz) | RF Duration (ms) |
|---|---|---|---|---|---|---|---|---|
| **a.** | | | | | | | | |
| HS | 4.0 | 741.9 | 5.0 | | | 850 | 1180.8 | 10.8 |
| | 6.0 | 754.9 | 5.0 | | | 850 | 1204.7 | 15.9 |
| | 8.0 | 759.0 | 5.0 | | | 850 | 1207.9 | 21.1 |
| | 6.0 | 754.9 | 7.5 | | | 850 | 1807.1 | 15.9 |
| | 6.0 | 754.9 | 10.0 | | | 850 | 2409.5 | 15.9 |
| | 6.0 | 754.9 | 12.5 | | | 850 | 3011.8 | 15.9 |
| | 6.0 | 754.9 | 15.0 | | | 850 | 3614.2 | 15.9 |
| | 6.0 | 714.9 | 10.0 | | | 900 | 2275.6 | 16.8 |
| | 6.0 | 677.3 | 10.0 | | | 950 | 2155.8 | 17.7 |
| | 6.0 | 643.4 | 10.0 | | | 1000 | 2048.0 | 18.7 |
| FOCI | 6.0 | 756.9 | 5.0 | 1.0 | 0.0 | 850 | 1204.7[a] | 15.9 |
| | 6.0 | 1138.2 | 5.0 | 2.0 | 0.0 | 850 | 3352.2[a] | 10.5 |
| | 6.0 | 1337.8 | 5.0 | 3.0 | 0.0 | 850 | 5519.0[a] | 9.0 |
| | 6.0 | 1476.6 | 5.0 | 4.0 | 0.0 | 850 | 7692.8[a] | 8.1 |
| | 6.0 | 1321.2 | 5.0 | 4.0 | 0.0 | 950 | 6883.0[a] | 9.1 |
| | 6.0 | 1195.3 | 5.0 | 4.0 | 0.0 | 1050 | 6227.5[a] | 10.0 |
| | 6.0 | 1091.4 | 5.0 | 4.0 | 0.0 | 1150 | 5686.0[a] | 11.0 |
| | 6.0 | 1004.1 | 5.0 | 4.0 | 0.0 | 1250 | 5231.1[a] | 12.0 |
| | 6.0 | 1330.6 | 5.0 | 4.0 | 1.0 | 850 | 6932.4[a] | 9.0 |
| | 6.0 | 1217.4 | 5.0 | 4.0 | 2.0 | 850 | 6342.6[a] | 9.9 |
| | 6.0 | 1126.4 | 5.0 | 4.0 | 3.0 | 850 | 5868.5[a] | 10.7 |
| **b.** | | | | | | | | |
| Default HS[b] | 4.0 | 741.9 | 5.0 | | | 850 | 1180.8 | 10.8 |
| Optimized HS | 6.0 | 643.4 | 10.0 | | | 1000 | 2048.0 | 18.7 |
| Optimized foci | 6.0 | 1168.3 | 3.0 | 4.0 | 1.2 | 950 | 3652.1[a] | 10.3 |

[a]Effective BW calculated using equation [7].
[b]Also used for STAR sequence.
BW, bandwidth; FOCI, frequency offset corrected inversion; HS, hyperbolic secant; RF, radiofrequency; STAR, signal targeting with alternating radio frequency.

For the first volunteer, the default settings of the HS labeling pulse were used and compared to the optimized HS and FOCI pulses. However, because severe off-resonance effects were observed with the default HS pulse (see Fig. 4), only the optimized HS and FOCI pulses were used for the other five volunteers. For these five volunteers, 4D-MRA using the STAR sequence was added for comparison. Table 1b shows the RF pulse parameters used for the first and other five volunteers.

All MR scans were performed on a Philips 3.0T Ingenia scanner (Philips, Best, The Netherlands) using a 32-channel head coil. Other imaging parameters were as follows: multi-shot multi-phase Look-locker readout, with 3D turbo field echo planar imaging (TFEPI) sequence (TFE factor of 13 in feet–head direction and EPI factor of 5 in right–left direction); field of view = 220 mm; scan matrix = $176 \times 176$, reconstructed as $256 \times 256$ by zero-filling; and 70 slices with thickness of 1.3 mm were acquired and reconstructed as 140 slices of 0.65 mm, sensitivity encoding (SENSE) factor = 2.3 in right–left direction and 1.2 in feet–head direction, echo time/repetition time = 4.9/13.0 msec, and flip angle = 10°. A total of 12 phase images (the first phase acts as the control image, and other 11 are labeled images) were acquired with an interval of 200 msec, resulting in PLDs between 49 msec and 2049 msec. The duration of the Look-Locker readout cycle was set to 2.4 seconds. Before starting the actual acquisition of the data, one dummy cycle consisting of 12 Look-Locker phases was performed to reach steady-state. Scan time was 3:40 min. Parameters for 4D-MRA using the STAR sequence were identical to the parameters of ACTRESS, except the number of phases being set to 11 to acquire the same number of subtracted image as ACTRESS MRA. The scan time of the STAR sequence was 6:50 minutes.

### Image Processing of In Vivo Data

First, magnitude subtraction of all labeled images (2nd–Nth phase; N = 12) from the control image acquired during the first phase of the sequence was performed. Maximum intensity projection (MIP) images for each temporal phase were generated in sagittal, transverse, and coronal directions.

To assess MT effects of the tested labeling pulses, the signal intensity of the background brain tissue on the subtracted images was measured through all temporal phases. For each volunteer, MIPs were produced across all temporal phases for each slice (temporal MIP), and two regions of interest (ROIs) were manually drawn on the left and right side of the brain on the 10th, 20th, 30th, 40th, and 50th slice, avoiding obvious vessels and artefacts. These 10 ROIs were copied to the original, non-MIP images, and the mean value was calculated as a function of PLD.

To investigate the relation between the labeling slab thickness and the bolus shape of the labeled blood, signal intensity in the M3 segment of both middle cerebral

arteries was measured. A MIP image across all phases in the transverse orientation was generated (4D-MIP). On one of them, two ROIs were manually drawn to indicate the M3. In these ROIs, 20 pixels with the highest signal intensity were chosen, and the mean signal intensity curves over all temporal phases were obtained.

Finally, a qualitative comparison of image quality and visualization of arteries was performed between ACTRESS-MRA and 4D-MRA acquired using the STAR sequence by a board-certified neuroradiologist with 12 years of experience (N.F.). The scoring system was as following:

- Visualization of peripheral arteries, superficial temporal artery (STA), and occipital artery (OA):
  4 = excellent, 3 = good, 2 = moderate, 1 = poor
- Noise from the background tissue and off-resonance artefacts:
  3 = almost no noise/artefacts, 2 = slight degree of noise/artefacts with no influence for diagnosis, 1 = certain degree of noise/artefacts with influence for diagnosis

## RESULTS

### Optimization of the Labeling RF Pulse

Table 1a shows the simulated values of BW and RF duration produced by changing the RF pulse parameters. When varying $\beta_{norm}$ while keeping $\mu$ and the RF integral fixed at default settings of 5.0 and 850, respectively, a higher $\beta_{norm}$ prolonged the RF pulse duration in a nearly linear relationship because the maximum $B_1$ amplitude was limited by that of the MRI scanner. Due to the concomitant increase in pulse duration, the increase of BW, which would help to reduce the off-resonance effects, was limited. Therefore, similar inversion profiles and off-resonance effects were observed for $\beta_{norm}$ of 4.0, 6.0, and 8.0 (Fig. 2a). For further optimization, $\beta_{norm}$ was set to 6.0 with a truncation level of 0.5% of the maximum HS amplitude and RF duration of 15.9 ms (for an RF integral of 850), both which are presumed not to generate degradation of the slice profile. A higher value of $\mu$ resulted in an increase of BW. However, the simulated inversion profile showed reduced labeling efficiency with higher $\mu$ (Fig. 2b), which can be counteracted by increasing the RF integral (Fig. 2c). Based on these results, $\beta_{norm}$ of 6.0, $\mu$ of 10.0, and an RF integral of 1,000, which resulted in RF duration of 18.7 ms, were used as the optimized HS pulse in the in vivo studies.

A higher value of $\alpha_{max}$ resulted in wider effective BW, although larger distortions were observed in the simulated inversion profile (Fig. 2d). These distortions were reduced with higher RF integral (Fig. 2e). The distortions also could be minimized (Fig. 2f) by increasing the level of the GG2. However, too high values in GG2 resulted in asymmetrical distortion when off-resonance effects were included in the simulations (Fig. 2g). Based on these observations, several combinations of RF parameters were tested in the preliminary study (data not shown), and the following parameters were determined as the optimized FOCI pulse for further investigation in the in vivo studies: $\beta_{norm} = 6.0$, $\mu = 3.0$, $\alpha_{max} = 4.0$, GG2 = 1.2, and RF integral = 950. Optimized RF parameters and simulated inversion profiles are shown in Table 1b and Figure 3 for comparison with the default settings.

### In Vivo Studies

Figure 4 shows that severe signal elevation was observed in off-resonant regions, such as tissue surrounding the paranasal sinuses and the petrous part of the temporal bone when the HS labeling pulse with the default settings was used. Similar artefacts only were present for the optimized HS pulses when a labeling slab of 200-mm thickness or thicker were employed. With the optimized FOCI pulses, no off-resonance artefacts were observed in any of the volunteers.

Figure 5a shows how the background static tissue signal varied over the readout phases for the different RF pulses, as measured in the first volunteer. Increased static tissue signal intensity was observed in the first few phases, which can be attributed to MT effects by the labeling pulse. These background signal changes were smaller for the optimized HS and FOCI pulses as compared to the HS pulse with the default settings. Figures 5b and c depict the averaged data over all six volunteers, showing that weaker MT effects were observed for a thinner labeling slab. This might be attributed to the stronger selection gradient employed for the thinner labeling slabs, which causes larger frequency offsets of the applied RF pulses.

Figure 5d shows the averaged signal intensity time courses, as measured in the M3 segment using the default HS, optimized HS, and FOCI pulses. The optimized HS and FOCI pulses generated very similar arterial signal, whereas the default HS pulse showed slightly lower signals during the peak of the bolus curve (Fig. 5d). For both optimized pulses (Figs. 5e and f), a thinner labeling slab of 80 and 100 mm resulted in lower maximum signal intensity, as well as smaller full-width half-maximum of the bolus curve. However, results from thicker labeling slabs of 160 and 200 mm did not differ significantly from the 120-mm labeling slab thickness, presumably due to the limited range of the body transmit coil.

The results of the qualitative comparison of image quality and visualization of arteries between ACTRESS-MRA and 4D-MRA using the STAR sequence are shown in Table 2, and Figure 6 shows example images from a representative volunteer. These images demonstrate that the ACTRESS approach can provide visualization of the dynamic passage of labeled blood flow through the vascular tree of a similar quality to the standard STAR sequence. This similar performance was corroborated by the observer study, which showed no difference in qualitative scoring measures between ACTRESS and the conventional ASL technique (STAR). Slightly reduced visibility of peripheral arteries was observed for ACTRESS-MRA, with thickness of 80- and 100-mm labeling slab thickness as compared to 120, 160, and 200 mm, as well as the STAR images. Similarly, labeling slab thicker than 120 mm did not have an obvious benefit for visualization of the STA, OA, or the peripheral

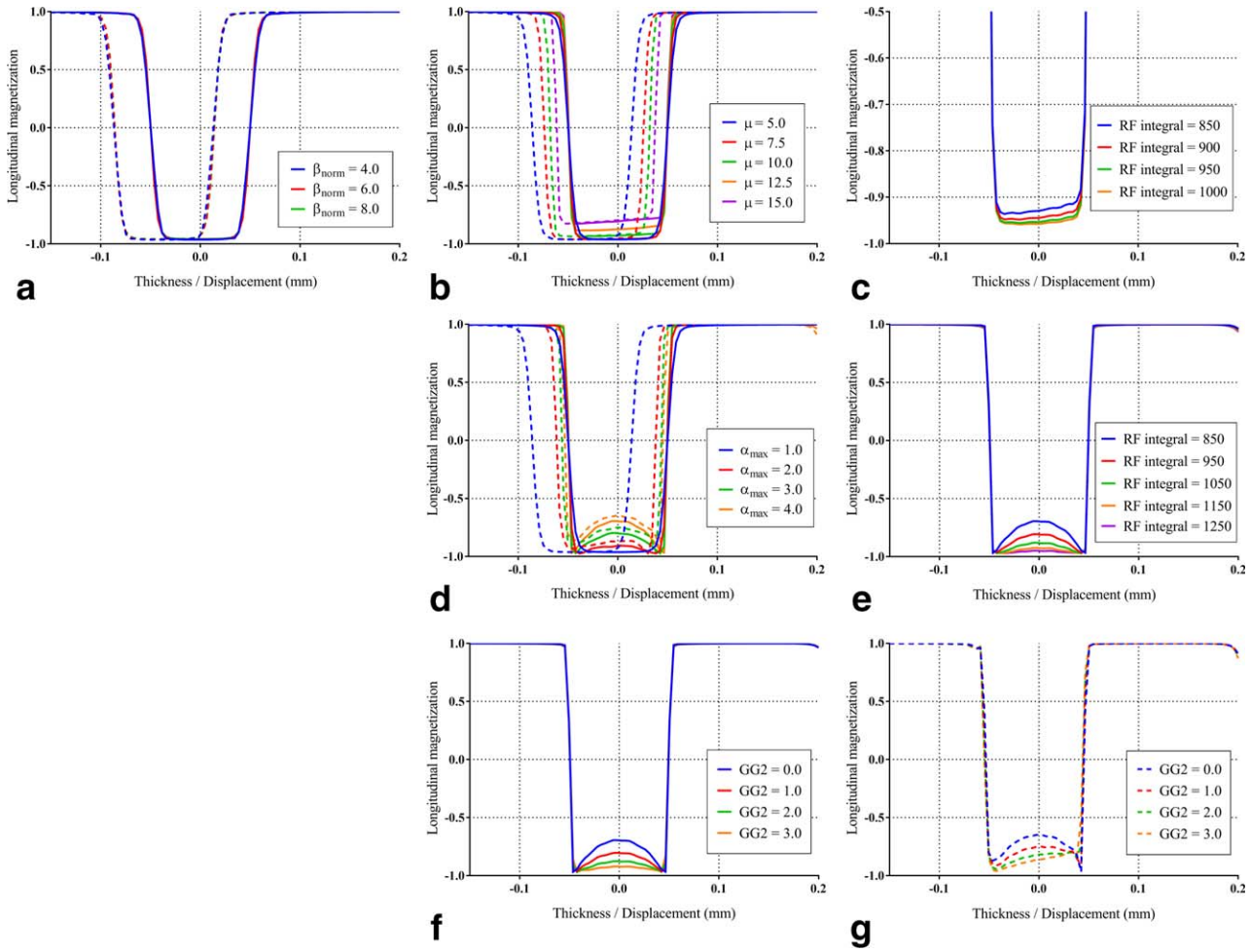


FIG. 2. Simulated inversion profile curves. (**a**) HS pulse, varying $\beta_{norm}$ with fixed $\mu$ and RF integral at default settings of 5.0 and 850. (**b**) HS pulse with varying $\mu$ ($\beta_{norm} = 6.0$, RF integral = 850). (**c**) HS pulse with varying RF integral ($\beta_{norm} = 6.0$ $\mu = 10.0$), (**d**) FOCI pulse with varying $\alpha_{max}$ ($\beta_{norm} = 6.0$ $\mu = 5.0$, RF integral = 850, GG2 = 0.0), (**e**) FOCI pulse with varying RF integral ($\beta_{norm} = 6.0$ $\mu = 5.0$, $\alpha_{max} = 4.0$, GG2 = 0.0), (**f**) FOCI pulse with varying GG2 ($\beta_{norm} = 6.0$ $\mu = 5.0$, RF integral = 850, $\alpha_{max} = 4.0$) at on-resonance, and (**g**) off-resonance of 3.4 ppm. For all graphs, solid line and dashed line represent on-resonance and off-resonance of 3.4 ppm, respectively. FOCI, frequency offset corrected inversion; HS, hyperbolic secant; RF, radiofrequency.

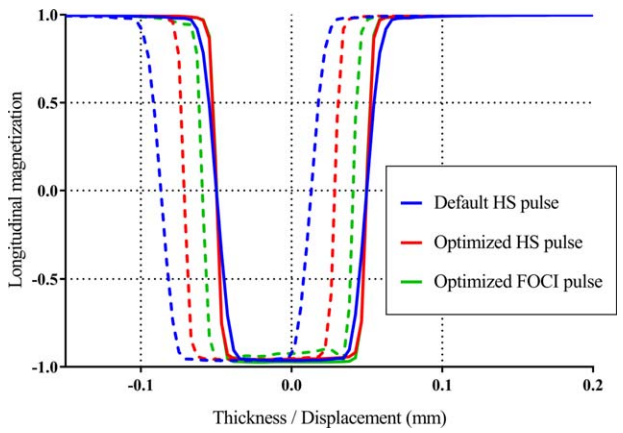


FIG. 3. Simulated inversion profile of HS pulse with default settings, optimized HS pulse, and optimized FOCI pulse. Solid line and dashed line represent on-resonance and off-resonance of 3.4 ppm, respectively. Radiofrequency parameters are shown in Table 1b. FOCI, frequency offset corrected inversion; HS, hyperbolic secant.

arteries as compared to the labeling slab of 120 mm. In fact, the visibility of OA was slightly weaker for ACTRESS-MRA for a labeling thickness of 160 and 200 mm as compared to 120-mm thickness.

In one of the five volunteers, slight motion was observed in the image acquired with the STAR sequence, resulting in reduced visibility of the peripheral arteries.

## DISCUSSION

In this study, we have presented a new ASL-based 4D-MRA technique, ACTRESS, which nearly halves the acquisition time of the conventional sequence by acquiring the labeled and control images in a single Look-Locker readout cycle. This brought down the typical acquisition time of a 4D-MRA sequence from approximately 7 to 3.5 minutes, which in clinical practice could be the difference between inclusion or exclusion of a 4D-MRA sequence in an examination protocol. We optimized the labeling RF pulse to minimize potential artefacts, and our observer

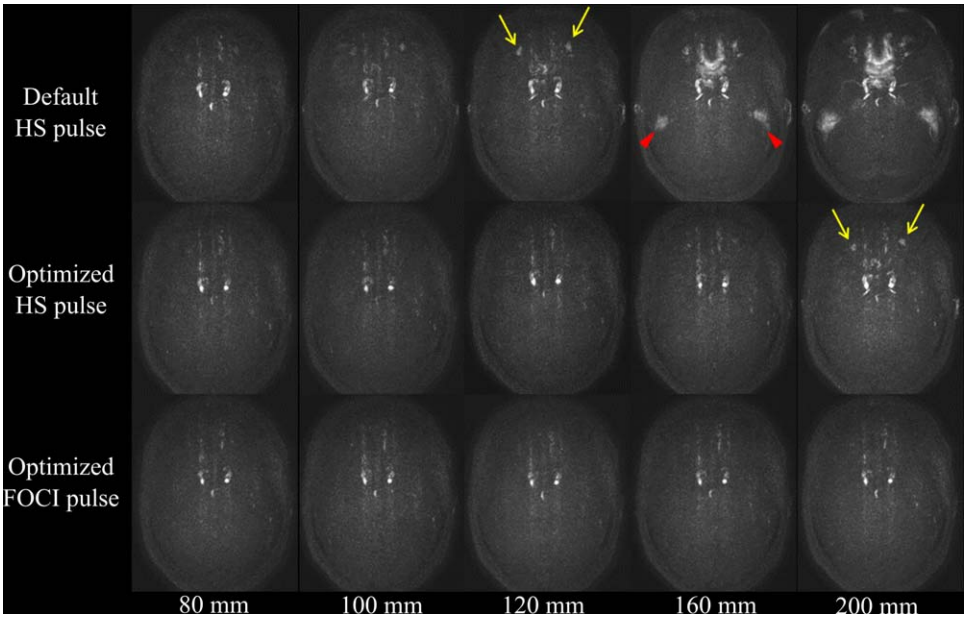


FIG. 4. Severe signal elevation was observed at tissue surrounding the paranasal sinuses (yellow arrows) and the petrous part of the temporal bone (red arrow heads) when the HS labeling pulse with the default settings was used. Similar artefacts were only present for the optimized HS pulses when 200-mm thick (or thicker) labeling slabs were employed. With the optimized FOCI pulses, no off-resonance artefacts were observed in any of the volunteers. FOCI, frequency offset corrected inversion; HS, hyperbolic secant.

study demonstrated that the ACTRESS-MRA achieved a very similar image quality to the standard ASL 4D-MRA.

To provide a comparable image quality to the standard ASL 4D-MRA, careful optimization of the labeling pulse was required. As compared to the HS pulse, the FOCI pulse with use of the Gaussian modulation allowed more flexible optimization. Because of the relatively low, maximally allowed $B_1$ amplitude of 13.5 μT of our clinical 3.0T scanner when using the body coil for RF pulse transmission, FOCI pulses with higher value of $\alpha_{max}$ showed a distorted inversion profile in the simulation results. Such distortions could be minimized by use of higher maximum $B_1$ amplitude, which is not allowed by the employed scanner, or by increasing the RF integral. However, these improvements would be achieved at the expense of increased MT effects. By applying the Gaussian modulation, the distortion of the inversion profile was reduced without a concomitant increase of MT

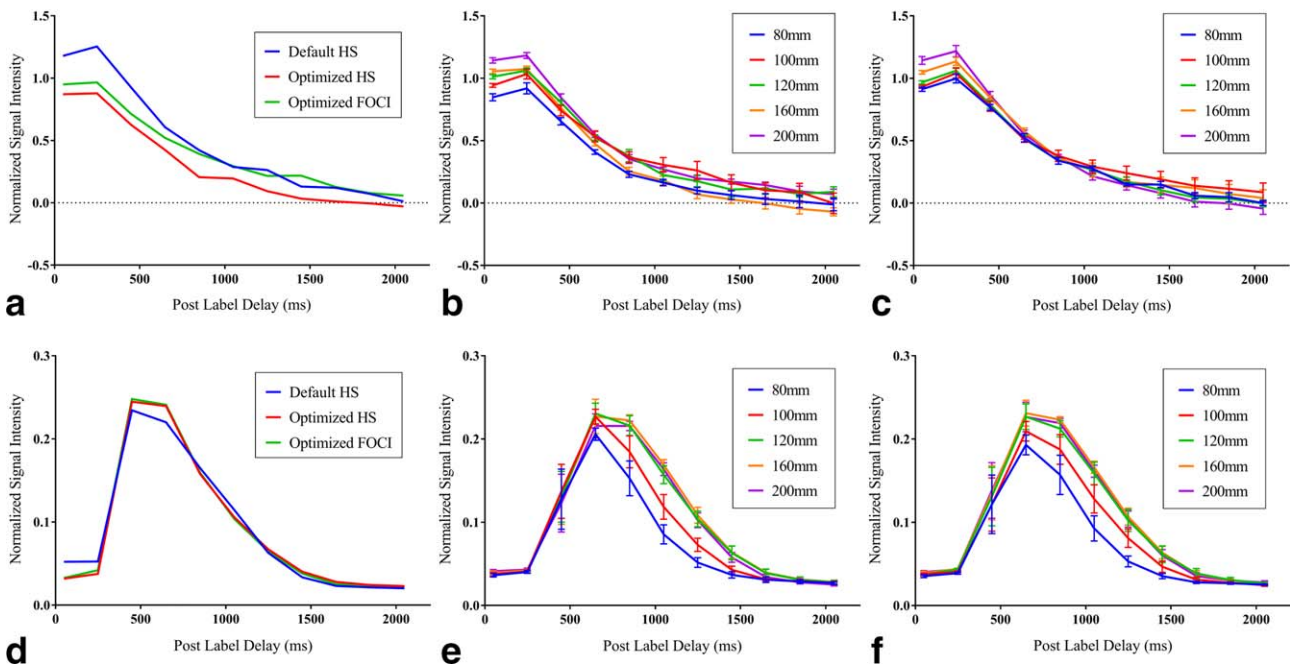


FIG. 5. Signal intensity curves over the readout phases acquired from in vivo study. (**a**) Background static tissue signal acquired with different RF pulses as measured in the first volunteer. (**b**) Averaged background static tissue signal over all six volunteers acquired with different labeling slab thickness of the optimized HS pulses and (**c**) optimized FOCI pulses. **d**) Arterial signal measured in the M3 segment using different RF pulses as measured in the first volunteer. (**e**) Averaged arterial signal over all six volunteers using the optimized HS pulses and (**f**) optimized FOCI pulses. FOCI, frequency offset corrected inversion; HS, hyperbolic secant; RF, radiofrequency.

Table 2
The Scores of the Qualitative Comparison of Image Quality and Visualization of Arteries between ACTRESS-MRA and Conventional 4D-MRA Using the STAR Sequence

| | Thickness (mm) | Visualization of Peripheral Arteries | Visualization of STA | Visualization of OA | Noise on the Background Tissue | Off-Resonance Artefacts |
|---|---|---|---|---|---|---|
| ACTRESS | 80 | 3.2 | 3.8 | 3.6 | 2.8 | 3.0 |
| (optimized HS) | 100 | 3.8 | 3.8 | 3.6 | 2.8 | 3.0 |
| | 120 | 4.0 | 3.8 | 3.6 | 2.8 | 3.0 |
| | 160 | 4.0 | 3.8 | 3.4 | 2.8 | 2.4 |
| | 200 | 4.0 | 3.8 | 3.4 | 2.8 | 1.6 |
| ACTRESS | 80 | 3.0 | 3.8 | 3.6 | 2.8 | 3.0 |
| (optimized FOCI) | 100 | 3.6 | 3.8 | 3.6 | 2.8 | 3.0 |
| | 120 | 4.0 | 3.8 | 3.6 | 2.8 | 3.0 |
| | 160 | 4.0 | 3.8 | 3.4 | 2.8 | 3.0 |
| | 200 | 4.0 | 3.8 | 3.4 | 2.8 | 3.0 |
| STAR | 300 | 3.8 | 3.8 | 3.8 | 2.8 | 3.0 |

ACTRESS, acquisition of control and labeled images in the same shot; HS, hyperbolic secant; MRA, MR angiography; OA, occipital artery; STA, superficial temporal artery; STAR, signal targeting with alternating radio frequency.

effects, although very strong Gaussian modulation induced asymmetrical distortions at off-resonance. Considering these observations and the fact that our ACTRESS approach is sensitive to MT effects, combination of the increase of RF integral and moderate Gaussian modulation was found to be optimal for the ACTRESS approach. Potentially, other adiabatic pulses such as BASSI-pulses (bandwidth-modulated adiabatic RF pulses for uniform selective saturation and inversion) (19) could achieve similar or even slightly better results, which could be tested for future implementations.

After the optimization of the labeling pulse, our in vivo study showed that the artefacts due to the off-resonance effects were minimized by increasing the BW of the HS labeling pulse, and completely annulled by use of the FOCI pulse. Furthermore, it was found that optimization of the labeling pulse was accompanied by a reduction of MT effects in the static tissue. For both

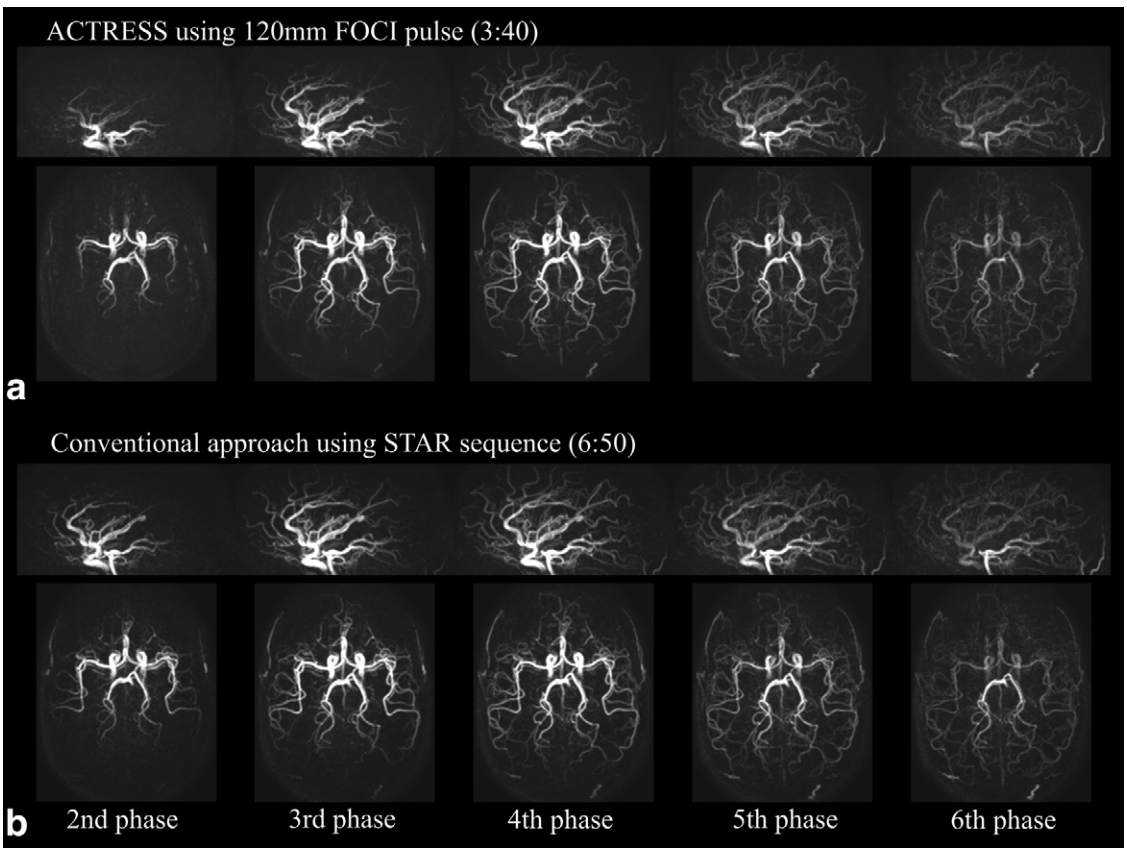


FIG. 6. Example images of ACTRESS-MRA and conventional 4D-MRA using the STAR sequence. ACTRESS, acquisition of control and labeled images in the same shot; FOCI, frequency offset corrected inversion; MRA, MR angiography; STAR, signal targeting with alternating radio frequency.

optimized HS and FOCI pulses, a wider range of frequency sweeps was applied to achieve a wider BW as compared to the default settings, and we can deduce that the MT effects within the imaging volume were reduced due to these larger frequency offsets. Control for MT effects is especially essential for perfusion imaging such that the signal intensity of the subtracted image reflects only the inflow of labeled arterial blood, hereby enabling accurate estimation of the cerebral blood flow (CBF). However, the prime goal of 4D-MRA is visualization of blood flow within the vasculature, which allows for some background signal to be present if it does not obscure visualization of the small vessels. The observer study demonstrated that the remaining MT effects for the optimized HS and FOCI pulses did not degrade visualization of peripheral arteries in ACTRESS-MRA. However, it should be noted that for now this approach is applicable only for 4D-MRA, whereas for perfusion imaging it will be difficult to use the same approach because it will be more sensitive to MT effects due to the much lower perfusion signal compared to the intensity of background tissue.

In our in vivo study, artefacts due to the off-resonance effects only were observed when using the optimized HS pulse with a slab thickness of 160 and 200 mm. Because the in vivo study indicated that the labeling slab with thickness of 160 and 200 mm did not provide any improvement in visualization, it seems there is no benefit of using a labeling slab thicker than 120 mm. Considering this fact, it can safely be said that the optimized HS pulse removed the off-resonance artefacts as effectively as the optimized FOCI pulse in our study. However, when subjects have relatively larger paranasal sinuses, it could cause larger off-resonance, and artefacts may appear even with a labeling thickness of 120 mm. To minimize the risk of artefacts, the use of FOCI pulses is recommended to achieve wider BW.

In the ACTRESS approach, it is assumed that the image acquired in the first phase does not have any labeled blood present to enable the use of the first phase image as the control image. However, this assumption could fail if the Look-Locker multi-phase acquisition is terminated before all labeled blood has disappeared from the arterial vessels by flow and/or decay of the labeling due to $T_1$ relaxation. If labeled blood were still present in the arterial vessels, this will cause reduced signal intensity from those arteries in the control image because the last phase of the Look-Locker readout is immediately followed by the first phase of the next Look-Locker readout cycle. Therefore, it is important to set the Look-Locker readout cycle duration long enough such that all labeled blood has flowed away or disappeared due to $T_1$ relaxation. This requires special attention in patients who have slow arterial flow and thus late arrival of label. Due to the cyclic properties of ACTRESS, an alternative way of presenting the technique would be that the last phase of the Look-Locker readout is used as control image with the label pulse played out just before the readout of the first Look-Locker phase. This alternative viewpoint might be helpful to understand the influence of slow flow on the 4D-MRA ACTRESS images.

The idea to minimize the influence of ASL pulses on the contrast of the control image to enable a shorter total acquisition time by minimizing the time spent on measuring control data has been mentioned previously in literature. An example of such an approach is the uninverted flow-sensitive alternating inversion recovery-technique (UNFAIR) (20). In this technique, spins in the imaging region experience 360-degree rotation by two inversion pulses for the label as well as the control condition. A small residual saturation of these spins will fully recover after a long enough PLD; the authors did suggest that any image acquired with the same imaging parameters without labeling pulse could serve as control image in this technique. However, this approach has not seen frequent application in recent literature or clinical protocols.

## CONCLUSION

A novel accelerated time-resolved ASL-MRA technique, ACTRESS, has been introduced. The labeling pulse was optimized to avoid artefacts due to off-resonance effects while also achieving a minor reduction of MT effects. Qualitative assessment demonstrated that ACTRESS-MRA is capable of producing a 4D-MRA image quality similar to conventional ASL 4D-MRA in close to half the scan time. This approach improves the clinical usability for many cerebrovascular diseases.

## REFERENCES


1. Yan L, Wang S, Zhuo Y, Wolf RL, Stiefel MF, An J, Ye Y, Zhang Q, Melhem ER, Wang DJ. Unenhanced dynamic MR angiography: high spatial and temporal resolution by using true FISP-based spin tagging with alternating radiofrequency. Radiology 2010;256:270–279.
2. Yan L, Salamon N, Wang DJ. Time-resolved noncontrast enhanced 4-D dynamic magnetic resonance angiography using multibolus TrueFISP-based spin tagging with alternating radiofrequency (TrueSTAR). Magn Reson Med 2014;71:551–560.
3. Iryo Y, Hirai T, Kai Y, Nakamura M, Shigematsu Y, Kitajima M, Azuma M, Komi M, Morita K, Yamashita Y. Intracranial dural arteriovenous fistulas: evaluation with 3-T four-dimensional MR angiography using arterial spin labeling. Radiology 2014;271:193–199.
4. Iryo Y, Hirai T, Nakamura M, et al. Collateral circulation via the circle of Willis in patients with carotid artery steno-occlusive disease: evaluation on 3-T 4D MRA using arterial spin labelling. Clin Radiol 2015;70:960–965.
5. Uchino H, Ito M, Fujima N, Kazumata K, Yamazaki K, Nakayama N, Kuroda S, Houkin K. A novel application of four-dimensional magnetic resonance angiography using an arterial spin labeling technique for noninvasive diagnosis of Moyamoya disease. Clin Neurol Neurosurg 2015;137:105–111.
6. Yu S, Yan L, Yao Y, et al. Noncontrast dynamic MRA in intracranial arteriovenous malformation (AVM), comparison with time of flight (TOF) and digital subtraction angiography (DSA). Magn Reson Imaging 2012;30:869–877.
7. Fujima N, Osanai T, Shimizu Y, Yoshida A, Harada T, Nakayama N, Kudo K, Houkin K, Shirato H. Utility of noncontrast-enhanced time-resolved four-dimensional MR angiography with a vessel-selective technique for intracranial arteriovenous malformations. J Magn Reson Imaging 2016;44:834–845.
8. Jensen-Kondering U, Lindner T, van Osch MJ, Rohr A, Jansen O, Helle M. Superselective pseudo-continuous arterial spin labeling angiography. Eur J Radiol 2015;84:1758–1767.
9. Gunther M, Bock M, Schad LR. Arterial spin labeling in combination with a look-locker sampling strategy: inflow turbo-sampling EPI-FAIR (ITS-FAIR). Magn Reson Med 2001;46:974–984.
10. Silver MS, Joseph RI, Hoult DI. Selective spin inversion in nuclear magnetic resonance and coherent optics through an exact solution of the Bloch-Riccati equation. Phys Rev A Gen Phys 1985;31:2753–2755.
11. Ordidge RJ, Wylezinska M, Hugg JW, Butterworth E, Franconi F. Frequency offset corrected inversion (FOCI) pulses for use in localized spectroscopy. Magn Reson Med 1996;36:562–566.

12. Norris DG. Adiabatic radiofrequency pulse forms in biomedical nuclear magnetic resonance. Concept Magnetic Res 2002;14:89–101.
13. Bernstein MA, King KF, Zhou XJ. Handbook of MRI Pulse Sequences. Burlington, MA: Elsevier Academic Press; 2004.
14. Payne GS, Leach MO. Implementation and evaluation of frequency offset corrected inversion (FOCI) pulses on a clinical MR system. Magn Reson Med 1997;38:828–833.
15. Yongbi MN, Branch CA, Helpern JA. Perfusion imaging using FOCI RF pulses. Magn Reson Med 1998;40:938–943.
16. Yongbi MN, Yang Y, Frank JA, Duyn JH. Multislice perfusion imaging in human brain using the C-FOCI inversion pulse: comparison with hyperbolic secant. Magn Reson Med 1999;42: 1098–1105.
17. Edelman RR, Siewert B, Darby DG, Thangaraj V, Nobre AC, Mesulam MM, Warach S. Qualitative mapping of cerebral blood flow and functional localization with echo-planar MR imaging and signal targeting with alternating radio frequency. Radiology 1994;192:513–520.
18. Stanisz GJ, Odrobina EE, Pun J, Escaravage M, Graham SJ, Bronskill MJ, Henkelman RM. T1, T2 relaxation and magnetization transfer in tissue at 3T. Magn Reson Med 2005;54:507–512.
19. Warnking JM, Pike GB. Bandwidth-modulated adiabatic RF pulses for uniform selective saturation and inversion. Magn Reson Med 2004; 52:1190–1199.
20. Helpern JA, Branch CA, Yongbi MN, Huang NC. Perfusion imaging by un-inverted flow-sensitive alternating inversion recovery (UNFAIR). Magn Reson Imaging 1997;15:135–139.